Surface and bulk electronic structure of ScN(001) investigated by scanning tunneling microscopy/spectroscopy and optical absorption spectroscopy

Hamad A. Al-Brithen and Arthur R. Smith
Condensed Matter and Surface Science Program, Department of Physics and Astronomy, Ohio University, Athens, Ohio 45701, USA

Daniel Gall
Department of Materials Science and Engineering, Rensselaer Polytechnic Institute, Troy, New York 12180, USA
(Received 20 June 2003; revised manuscript received 1 March 2004; published 6 July 2004)

ScN(001) 1×1 surfaces have been prepared by growing ScN on MgO(001) using radio frequency molecular beam epitaxy. *In situ* ultrahigh vacuum scanning tunneling spectroscopy indicates that the Fermi level at the surface lies slightly above the Sc 3*d* conduction band edge, which is attributed to a downward band bending at the surface. *In situ* scanning tunneling microscopy is used to image the Sc and N atom sublattices. While only one atom (Sc) appears at small negative bias, both atoms (Sc and N) appear at certain positive sample biases due to the partially ionic nature of the bonding. Charge accumulation near ionized subsurface donors is evident from the long-range topographic distortions at the surface. The combination of tunneling spectroscopy and optical absorption results show that ScN has an indirect bandgap of 0.9 ± 0.1 eV and a direct transition at 2.15 eV.

DOI: 10.1103/PhysRevB.70.045303 PACS number(s): 73.20.At, 68.35.Bs, 68.37.Ef, 78.66.Fd

I. INTRODUCTION

Transition metal nitrides (TMN's) have been receiving a lot of interest for their unique physical properties including high hardness, high-temperature stability, mechanical strength, off-stoichiometry, magnetic properties, and electronic transport properties that vary from semiconducting to metallic.[1–14] One TMN of great interest, due to its unique properties and potential applications, is ScN. Scandium can be combined with nitrogen to form a rocksalt compound with lattice constant $a_{\mathrm{ScN}}=4.501$ Å, hardness $H\sim21$ GPa, and melting point $T_m\sim2600\,^{\circ}\mathrm{C}$.[7–9,12,15–18] A very small mismatch in the lattice constants between ScN and *c*-GaN suggests the interesting possibility of forming either ScN/GaN heterojunctions or ScGaN alloys.[19–21] The rocksalt structure of ScN is attributed to the bonding between Sc and N being partially ionic.[22] Early theoretical work reported that ScN had a semimetallic electronic structure.[23–25] However, new theoretical work concludes that ScN is instead a semiconductor with a direct optical transition at the *X* point between 2 and 2.9 eV. An indirect transition from $\Gamma\rightarrow X$ below the direct one is also expected in the range 0.9–1.6 eV.[6,11,26] Experimental reports have determined that a direct transition lies in the range 2.1–2.4 eV.[8,9,15,19,27,28]

The possible indirect transition and other issues regarding ScN have been difficult to address experimentally due to various complications in growing the films, such as the difficulty to grow ScN having a specific crystalline orientation, and the difficulty to obtain a film having a smooth surface. Bai *et al.* grew ScN using a variety of growth methods, such as reactive sputtering from a Sc-metal target in a pure nitrogen atmosphere. This resulted in ScN films having various crystal orientations, depending on the growth method used and the type of substrate.[15,16] Gall *et al.* showed that the growth of ScN on MgO(001) using ultrahigh-vacuum reactive magnetron sputter deposition resulted in an epitaxial single crystal ScN(001) film if a specific substrate bias or a TiN buffer layer was applied; otherwise, ScN(111) would also form.[1,9,10]

Shortly after this, Al-Brithen *et al.* showed that the growth of ScN on MgO(001) using rf MBE resulted in an epitaxial film having very high crystalline quality, single (001) orientation, and atomically smooth surface terraces.[18] The stoichiometry of the ScN(001) grown film using rf MBE was later shown to depend on the flux ratio $J_{\mathrm{Sc}}/J_{\mathrm{N}}$, during growth.[8] If the growth is under scandium rich conditions, the bulk Sc/N ratio (measured as high as 1.00:0.83) approximately equals the flux ratio $J_{\mathrm{Sc}}/J_{\mathrm{N}}$ during growth, but the rocksalt structure is maintained, resulting in growth with nitrogen vacancies.[7,8] If the growth is under nitrogen rich conditions, N vacancies are suppressed and the material is close to stoichiometric (1:1).

In prior work, Al-Brithen *et al.* succeeded in imaging one of the surface atom sublattices of ScN(001) 1×1 but did not determine if those atoms were Sc or N.[18] Subsequent theoretical work by Takeuchi *et al.* and also Stampfl *et al.* found that the energetically most stable surface structure of ScN(001) in N-rich conditions is the ideal, bulklike surface; they also presented simulated STM images showing Sc and N atoms at different biases.[29,30] To compare with experiments, however, it is essential to know the actual surface bandgap and Fermi level position. Therefore, it remains to be shown experimentally what atom on the ideal ScN(001) 1×1 surface is imaged in STM and how that relates to the electronic structure.

In this paper, *in situ* ultrahigh vacuum (UHV) STM and scanning tunneling spectroscopy (STS) are combined with optical absorption spectroscopy to study the surface and bulk electronic structure of ScN(001) and to identify the surface atoms imaged in STM as a function of sample bias voltage. As well, we address the indirect bandgap issue.

II. EXPERIMENTAL PROCEDURE

ScN layers are grown by molecular beam epitaxy (MBE) on MgO(001), using a radio frequency (RF) plasma source for nitrogen and an effusion cell for scandium. Details of the MBE growth setup and substrate cleaning procedure are published elsewhere.[8,18] ScN growth takes place with the substrate set at $\sim 800\,^{\circ}\mathrm{C}$ and the pressure of nitrogen and plasma source power set at 9×10^{-6} Torr and 500 W, respectively.

The growth starts when the scandium shutter is opened. Scandium (nitrogen) rich growth conditions occur when the Sc flux J_{Sc} (N flux J_N) exceeds the N flux J_N (Sc flux J_{Sc}).[7,8] The average scandium flux J_{Sc} is determined by measuring the final film thickness using a thickness profilometer; from this, and by knowing the growth time and Sc atomic density in ScN, the Sc flux J_{Sc} is calculated. The effective N flux is determined to be $J_N \sim 3.6\times 10^{14}\ \mathrm{cm}^{-2}\ \mathrm{s}^{-1}$ in our system for the stated conditions.[7,8] The flux ratio (J_{Sc}/J_N) can be adjusted by changing the scandium effusion cell temperature.

The growth is monitored in real time using RHEED. Following growth, samples are transferred under vacuum to the scanning tunneling microscope chamber for *in situ* surface analysis. STM tips are prepared by electrochemical etching in a NaOH solution followed by dipping in H_2O to remove residual hydroxides. After loading into the STM chamber, electron beam heating using a tip bias of +160 V and an emission current of $\sim$1.5 mA for a period of about 20 min is used to clean the tips prior to use.

After removing the sample from the chamber, the metal backing of the substrate is removed, leaving just the ScN film on the MgO (bandgap $\sim$8 eV) substrate. Optical analysis was performed using a Varian CARY UV-VIS-NIR two-beam photospectrometer with a wavelength range from 176 to 3300 nm. Transmission spectra were obtained by placing the sample directly in the beam while reflection data was acquired in a W geometry, using an Al mirror which was calibrated with the identical beam path and measurement settings as used for the reflection measurements. The overall uncertainty in the reflection and transmission spectra is less than 2% and is primarily due to sample positioning errors and diffuse scattering from the back surface of the MgO substrate.

III. RESULTS AND DISCUSSION

A. Scanning tunneling microscopy of ideal bulklike ScN(001) 1×1

It is widely known that, in the case of covalent compound semiconductor surfaces, the anion is imaged at negative sample biases (filled states) while the cation is imaged at positive sample biases (empty states). This principle of atom selective imaging was demonstrated conclusively by Feenstra *et al.* in the case of the GaAs(110) surface.[31] Following this rule in the present case of ScN(001) 1×1, the majority band of states in the valence band (VB) should be the N 2*p* states, while the majority band of states in the conduction band (CB) should be the Sc 3*d* states. However, as has been shown by several recent theoretical works, since the bonding is partially ionic, there is a minority band of Sc 3*d* states in the VB and also a minority band of N 2*p* states in the CB.[6,11,29] For example, the N atoms have also some empty character, and the Sc atoms have also some filled character. Since for our sample the Fermi level is close the CB (as will be shown by the STS results), STM images are expected to show mainly the cations (Sc atoms) but possibly also the anions (N atoms).

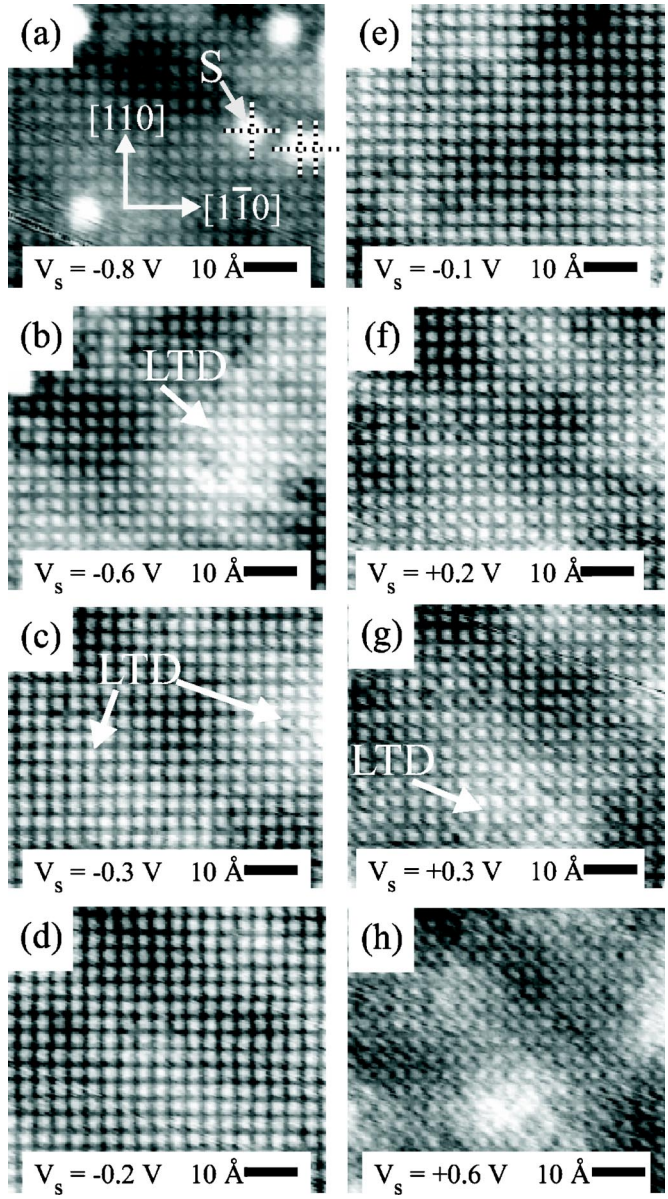

FIG. 1. STM images of a ScN(001) 1×1 surface grown under N-rich conditions acquired at different sample biases. The gray scale ranges are (a) 0.7, (b) 0.35, (c) 0.38, (d) 0.38, (e) 0.38, (f) 0.27, (g) 0.31, and (h) 0.31 Å, respectively. The tunneling current was set at 0.1 nA. Crosses are marked at the centers of the S features.

We note that density functional calculations predict that the N atoms of this surface are buckled upward by $\sim$0.02 Å compared to the Sc atoms, resulting in a relaxed but unreconstructed surface.[29,30] However, 0.02 Å is a small difference, and electronic effects may totally dominate geometrical effects in STM images. The proof of the chemical identifica-

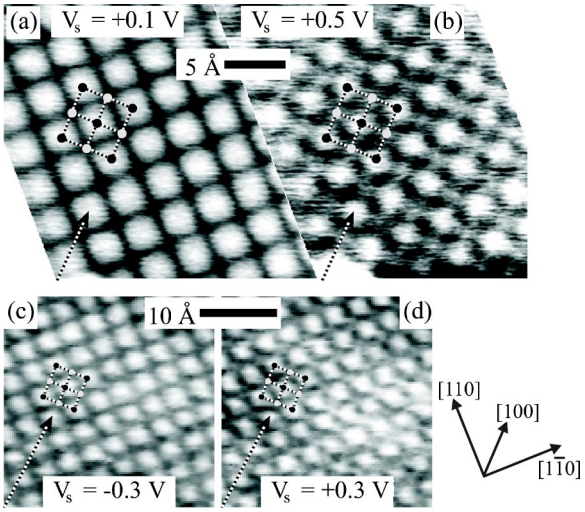

FIG. 2. Dual bias STM images of ScN(001) 1×1 surface grown under N-rich conditions. (a) $V_S=+0.1$ V; (b) $V_S=+0.5$ V; (c) $V_S=-0.3$ V; (d) $V_S=+0.3$ V. Tunneling currents for (a)–(d) are 0.1 nA. The gray scale ranges are 0.28, 0.13, 0.32, and 0.23 Å for (a)–(d), respectively.

tion will therefore require the results of STS.

1. Bias dependence of sublattice protrusions

Figure 1 shows STM images of the ScN(001) 1×1 surface grown under N-rich conditions as a function of sample bias voltage. All images belong to the same terrace, but not exactly the same area due to thermal drift effects.

As seen in Figs. 1(a)–1(h), the images are mainly composed of a square array of prominent protrusions which are clear at all displayed sample biases, from $V_S=-0.8$ to +0.6 V. The spacing of these protrusions is ~3.2 Å, corresponding to the spacing along [110] between atoms of the same type on a bulklike ScN(001) 1×1 surface. The minimum observed step height between adjacent terraces was previously determined to agree with the ScN(001) interplanar spacing.[18] Upon crossing a single monolayer height step, the atomic rows shift by one-half the row spacing, as expected if the prominent atomic row directions are along ⟨110⟩. It will be shown below that these most prominent protrusions correspond to the Sc atoms.

As V_S increases above $\sim+0.3$ V, Figs. 1(g) and 1(h), within the same image a second array of smaller protrusions begins to appear in addition to the primary protrusions. These smaller protrusions, mainly visible in Fig. 1(h) at $V_S=+0.6$ V, clearly correspond to the sublattice opposite to that of the prominent protrusions, and it will be shown below that these lesser protrusions correspond to the N atoms. At higher sample biases $V_S>+0.6$ V, the atomic corrugation of the STM images (not shown) becomes increasingly weaker due to increased tip-sample separation.

At $V_S=-0.8$ V, we observe the appearance of several bright spots in the STM image, denoted *S*, which are centered on the smaller protrusion sublattice (N) sites, as seen in Fig. 1(a); these localized features extend over approximately four neighboring prominent protrusion (Sc) sites. We have not seen these features at other sample biases. One possibility is that they are O or CO adsorbates which attach to the four neighboring Sc atoms. In Fig. 1(a) we count six S sites out of about 340 surface sublattice sites, so the coverage is ~1.8%.

As seen in Fig. 2, simultaneous dual-bias imaging was also performed on an identical surface area at bias voltages of $V_S=+0.1$ V [Fig. 2(a)] and $V_S=+0.5$ V [Fig. 2(b)] with tunneling current set at $I_T=0.1$ nA. This ScN(001) surface was prepared under N-rich conditions, similarly to that of Fig. 1. At $V_S=+0.1$ V, the sublattice of prominent atomic (Sc) protrusions, whose row directions are along ⟨110⟩, is clearly visible. At $V_S=+0.5$ V, these prominent atomic (Sc) protrusions appear reduced in size compared to those at +0.1 V, likely due to the increased tip-sample separation, while the opposite sublattice of smaller (N) protrusions appears clearly. The Sc-N-Sc-N chain directions of the rocksalt structure are along ⟨100⟩.

Dual-bias images acquired at $V_S=-0.3$ and +0.3 V are also displayed in Figs. 2(c) and 2(d), respectively. Here it is clearly seen that there is no shift in the position of the prominent atomic protrusion between these two biases. These main protrusions correspond to the Sc atomic sites. At +0.3 V in Fig. 2(d), the N sites are faintly visible.

2. Charge accumulation

It is also noticed in most of the images of Fig. 1(a) some areas which are brighter compared to the surrounding area. These bright areas are seen at all displayed sample biases, several of which are labeled in Fig. 1 as LTD (long-range topographic distortion). Similar effects have been seen in STM images of GaAs(110) surfaces by Stroscio *et al.*, Zheng *et al.*, and Chao *et al.* in the case of *n*-type, *n*-type, and *p*-type samples, respectively.[32–34] It has been shown that for GaAs(110) surfaces that these LTD's, as they have been referred to, are due to the presence of either ionized dopant impurities within the top five or six atomic layers[33,34] or to charged surface adsorbates.[32] Zheng *et al.* and Chao *et al.* even categorized the apparent brightness according to which subsurface layer the ionized dopant occupies.[33,34]

In the present case of rocksalt ScN(001), also a nonpolar, relaxed surface, we give a similar interpretation to the observed bright patches. It will be shown (below) from the spectroscopy measurements that the sample is highly *n* type (4.8×10^{18} cm^{-3}). This high *n*-type conductivity is attributed to O_N's and/or nitrogen vacancies (V_N's), both of which can act as donors in ScN.[8,21,26,35] Although for N-rich growth, Stampfl *et al.* found that the V_N formation energy for N-rich conditions is very high (4.32 eV),[30] growth kinetic limitations might still result in some V_N's. Moreover, O_N's could occur; one source of oxygen could be diffusion from the substrate, MgO. Another possibility could be trace oxygen impurities from the sources. Whether from V_N's or O_N's, the bright patches seen in Fig. 1 are attributed to the effects of ionized subsurface donors. Since these ionized donors are positively charged, they attract to their vicinity free conduction electrons, resulting in local accumulation of electron density which appears in the STM images as the bright

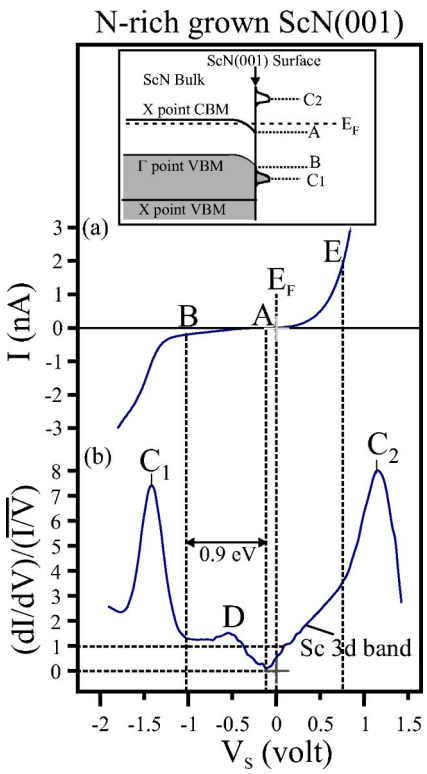

FIG. 3. Averaged tunneling spectroscopy results for the ideal, bulklike ScN(001) surface grown under N-rich conditions: (a) current vs voltage; (b) normalized conductivity vs voltage. Inset is a band diagram showing Fermi level position relative to conduction band and band bending near the surface.

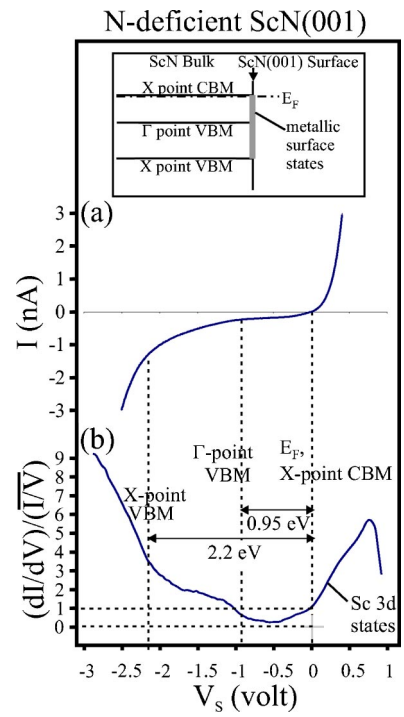

FIG. 4. Averaged tunneling spectroscopy results for the Sc-rich ScN(001) surface grown under Sc-rich conditions: (a) current vs voltage; (b) normalized conductivity vs voltage. Inset is a band diagram showing Fermi level position relative to conduction band.

patches. The spectroscopy (next section) suggests that this accumulation is accompanied by a downward band bending of a few tenths of an eV.

B. Scanning tunneling spectroscopy of ScN(001) surfaces

In this section, the tunneling spectroscopy of ScN(001) surfaces acquired under UHV conditions is discussed, first for the N-rich case. This is followed by a discussion of dopant-induced band bending, then by the identification of the surface atoms seen in STM images for the ideal 1×1 surface. After that, the tunneling spectroscopy is discussed for the N-deficient surface. In Figs. 3 and 4, the upper panels [Figs. 3(a) and 4(a)] display measured current vs voltage, (I-V) curves while the lower panels [Figs. 3(b) and 4(b)] display the normalized conductance $(dI/dV)/(\overline{I/V})$ vs voltage, (NC-V) curves, numerically calculated from the I-V data of the upper panels. Normalized conductance (NC) is in general well known to be proportional to the surface local density of states (LDOS), and here we calculate it following the method described by Feenstra.[36] The bar over the I/V indicates broadened I/V values are used to avoid divergences near the band edges.[36] The horizontal dashed lines in the (NC-V) panels indicate where NC equals zero and unity. All sets of spectra were acquired using tungsten tips with a fixed tip-sample separation for each spectrum. Graphs 3(a) and 4(a) are the results of averaging over 16 and 10 STS spectra, respectively.

1. Tunneling spectroscopy of ideal bulklike ScN(001) 1×1 surface

Figure 3 shows the I-V and NC-V curves for a stoichiometric ScN(001) surface grown under N-rich conditions having an atomically well-ordered surface structure similar to the ones shown in Figs. 1 and 2. In Fig. 3(a), the current on the negative sample bias side slowly becomes more negative over a range of about one volt and then turns sharply down, whereas on the positive sample bias side it increases exponentially from near zero volts. Since positive sample bias corresponds to electrons tunneling *into* the sample, thus into the empty or conduction band (CB) states, the I-V behavior is consistent with a semiconductor where the Fermi level (E_F) is close to the CB. This indicates that the sample is highly n type ($n=4.8\times10^{18}$ cm^{-3}, see optical absorption analysis, below), and it has important consequences for determining which atoms (Sc or N) are imaged in STM.

As seen in Fig. 3(b), the NC is close to zero at its minimum (point A which occurs near $V_S=-0.1$ V), which suggests that this surface is a semiconductor (Note: in absence of band bending this minimum would occur at E_F). As V_S increases over the range -0.1 to 0.75 V (point A to point E), the NC increases approximately linearly with V_S. Such linear behavior is in excellent agreement with bulk calculations which find a linearly increasing DOS with energy for the Sc 3d states in the lower part of the CB near the X point.[11] Also, surface calculations show the same linear behavior for the Sc 3d 1×1 surface LDOS.[29] Thus, the linear relation of the NC-V curve in the bias range from ~-0.1 to 0.75 V is attributed to the Sc 3d states with the conduction band mini-

mum (CBM) at the X point 0.1 eV below E_F.

At the point E ($V_S = +0.7$ V), there is another turn-on leading to the peak C_2. We associate this peak with a Sc derived surface state (actually a surface resonance since it lies within the bulk CB).

As V_S decreases from −0.1 V, we find a hump at point D. Since the position of this D feature with respect to the CB edge varies with position on the surface, it is evidently not an intrinsic ScN state. While it could be an extrinsic state, similar features have been seen by Feenstra for the clean, nonpolar surfaces of several III-V semiconductors.[36] In those cases of n-type conductivity, the "dopant-induced" features are due to electrons tunneling out of filled states near the bottom of the CB into empty states of the tip. This tunneling occurs even for very small negative sample biases, giving the appearance of a very small energy gap. Feenstra reported that observation of the dopant-induced component is an indicator of high surface quality.[36] In the case of the nonpolar ScN(001) 1×1 surface which is heavily n type, substantial dopant-induced tunneling is possible. The D feature can therefore be attributed to this effect.

At $V_S \sim -1.0$ V in Fig. 3(b), a strong onset appears at the point B. In other sets of data (not shown), while the position of the CBM varies by 0.1–0.2 eV, we find that the voltage difference from point A to point B is constant, indicating an intrinsic ScN bandgap with the point B at the valence band maximum (VBM). Therefore, we find an energy gap at the surface $\Delta E_{g,\min} = e(V_A - V_B) \sim 0.9$ eV. The value of $\Delta E_{g,\min}$ is much smaller than the measured direct gap of ScN (2.1–2.4 eV);[8,9,15,19,27,28] however, it is within the range of the predicted indirect gap for ScN (0.9–1.6 eV)[6,11,26] suggesting that the point B corresponds to the theoretically predicted VBM at the Γ point. Below the B onset lies a peak at C_1. This peak can be interpreted as a N derived surface state (surface resonance). For Fig. 3, the data range does not extend far enough to reach the onset of the VBM at the X point.

2. Origin of long-range topographic distortion: Band bending on ScN(001)

Spectroscopy from different surface areas shows that the Sc 3d states extend below E_F by 0.1–0.3 eV. One possible explanation is that the Sc 3d surface LDOS is shifted to lower energies compared to the bulk. Yet, according to Takeuchi *et al.*, the surface LDOS is very similar to that of the bulk, and surface relaxation results in only a small energy gain of 0.03 eV/1×1 cell compared to the nonrelaxed surface.[29] Moreover, the calculations of Stampfl *et al.* indicate that the ScN(001) surface has no states inside the band gap.[30]

Estimating from the theoretical electron band effective mass $m^* = 0.281 m_e$,[37] and experimental dielectric constant $\varepsilon \sim 7.2$,[11] we calculate a donor ionization energy of approximately 74 meV using the hydrogenic model. From the results of our optical studies (below) we get a carrier concentration of 4.8×10^{18} cm^{-3}, but we do not know the (unintentional) dopant concentration. However, since the material is high n type, E_F should lie close to the CB in the bulk, as indicated schematically in the inset of Fig. 3(a). Moreover, the absorption spectrum (discussed below) indicates that the material is semiconducting, so the Fermi level should lie below the CB edge in the bulk. The STS spectroscopy on the other hand shows that E_F at the surface is 100–300 meV above the CBM. This can be explained by a downward band bending at the surface.

A downward band bending in the vicinity of the bright LTD's seen in Fig. 1 is also expected. These LTD's, corresponding to electron accumulation, can be explained as due to a lowering of the band edge caused by the Coulomb field of the subsurface ionized donors, as was explained for the case of n-type GaAs(110).[33] We also find that the amount of band bending varies from spectrum to spectrum as it should since it depends on where on the surface the spectrum was acquired. We further note that observing the LTD's as raised features at both positive and negative sample biases is due to E_F being inside the CB at the surface in the vicinity of those features. For either positive or negative sample bias, the greater band bending near the LTD regions results in a larger integrated LDOS compared to the surrounding area. For a constant current image, this results in the tip retracting slightly, causing the bright areas in Fig. 1.

3. Identification of sublattice atoms for ideal bulklike ScN(001) 1×1 surface

The STM image is determined by the integral over those states between E_F and $E_F + e\times V_S$. Since for the ideal 1×1 surface with high n-type doping there are Sc 3d states both above and below E_F as has been shown, for any small sample bias either positive or negative, the tunneling current will contain a large contribution from the Sc 3d states. Even for bias voltages <-0.1 V, the tunneling current will still include the Sc 3d contribution, and only the dopant induced contribution begins to be added (states labeled D in Fig. 3). Thus, within the sample bias voltage range −0.8 to +0.6 V, the primary protrusions must be the Sc atoms.

At sufficient positive sample bias ($>+0.3$ V), the N sublattice begins to appear [see Figs. 1(h) and 2(b)]. This indicates that N derived states exist within the Sc 3d CB, as has been predicted by Takeuchi *et al.* who also showed both Sc and N atoms in their gray plots of the LDOS at $V_S = +1.0$ V.[29]

According to the LDOS calculations of Takeuchi *et al.*, the upper part of the VB is composed primarily of N 2p derived states but also a small contribution of Sc 3d states. Those authors therefore showed gray plots at negative sample bias, finding both Sc and N atoms at $V_S \sim -0.5$ V and primarily N atoms at $V_S \sim -1.0$ V. But this was assuming almost no surface gap (underestimated). As seen in the NC -V spectrum of Figs. 3(b), the N 2p states only begin to appear for $V_S < -1.0$ V. In our earlier paper,[18] we reported that only a small relative shift, much less than the expected $a/2$, was observed in dual bias images recorded at sample biases of +1.0 and −1.0 V. This is now understood since the Sc 3d states are dominant for our n-type sample over the range −1.0 to +1.0 V.

Stampfl *et al.* also made simulated STM images for sample bias voltages of −2.0 and +2.0 V, which showed N atoms and Sc atoms, respectively, but not both types of atoms at the same bias. They also found a surface gap using a

screened-exchange LDA approach, with surface states outside the bulk gap. We cannot make direct comparison to their simulated images since we did not achieve atomic resolution images at such large magnitudes of voltage.

4. Tunneling spectroscopy of N-deficient ScN(001) surface

The N-deficient ScN(001) surface is prepared by growth under Sc-rich conditions. The resulting bulk structure is composed of a complete Sc sublattice but a N sublattice having V_N's in proportion to the excess Sc flux during growth.[8] The crystal structure remains rocksalt, and the bulk V_N's make the film highly *n*-type with carrier densities on the order of 10^{21} cm^{-3}.[8] Concerning the surface from calculations, Stampfl *et al.* found that a 2×1 N-vacancy structure was energetically most favorable under Sc-rich conditions; also the Sc-terminated structure was not too much higher in energy.[30] There are many states in the bulk gap, making the surface metallic. Takeuchi *et al.* also found a metallic surface structure with new surface states close to E_F.

Our STM images of the Sc-rich grown surface show qualitative good agreement with the calculations, although no well-ordered surface structure is observed; however, smooth terraces and single atomic height steps are clearly visible.[7] This surface also shows a clearly lower surface adatom diffusion barrier (by 0.26 eV) compared to the stoichiometric surface, which is attributed to the weaker Sc-Sc bonding (metallic) compared to Sc-N bonding (covalent/ionic).[7,8] It was concluded that this surface contains an excess of Sc metal, with up to 100% N vacancies.[7]

The main advantage of doing tunneling spectroscopy on this surface is that, because of the Sc-rich (N-deficient) surface structure, the N derived surface state should be absent. This may allow us to isolate the bulk projected valence band states. Figure 4 shows the tunneling spectroscopy results for ScN(001) grown under Sc-rich conditions. Figure 4(a) shows that the current increases exponentially with positive sample voltage from near the Fermi level. Figure 4(b) shows that the derived normalized conductance has the expected CB linear relation with voltage starting at $V_S=0$ V up to at least $\sim+0.4$ V, similar to the stoichiometric case [Fig. 3(b)]. The value of the NC at E_F is close to unity, consistent with a metallic surface. The peak near $V_S=+0.7$ V is attributed to a Sc derived surface peak.

The turn-on of states near the Fermi level indicates that the X point CB onset is near E_F, as indicated in the band diagram shown in the inset of Fig. 4. The valley of states between $V_S=0$ and -0.9 V is attributed to metallic or defect states within the bandgap. It can also be noticed that the N derived surface state peak C_1 seen for the stoichiometric surface [Fig. 3(b)] is absent for the N-deficient surface [Fig. 4(b)]. A band onset, consistent with the theoretically predicted VBM at the Γ point, is observed at $V_S\sim-0.95$ V, and therefore, we find a bandgap E_g of ~0.95 eV. Another band onset, consistent with the theoretically predicted VBM at the X point, is observed near $V_S\sim-2.2$ V. With the CBM near 0 V, the energy difference between the onset and the CBM is consistent with reported values for the direct transition at the X point in the range 2.1–2.4 eV and in excellent agreement with our own measured value of 2.15 eV.[8,9,15,19,27–30]

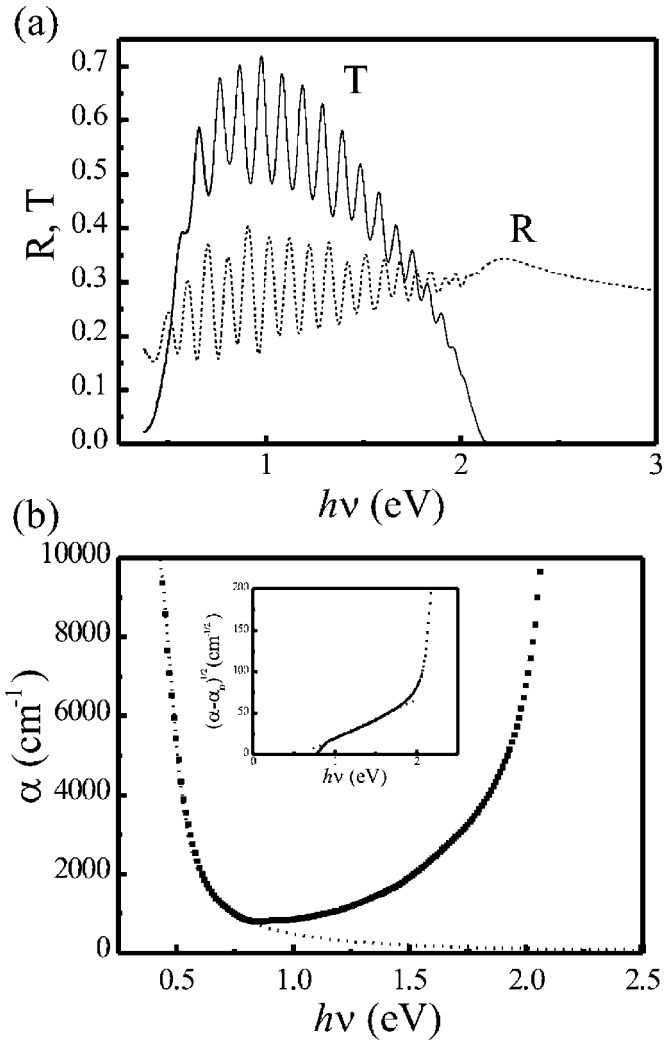

FIG. 5. (a) Reflection and transmission coefficients R and T as a function of photon energy $h\nu$ acquired for a 2.5 μm thick ScN film grown under N-rich conditions; (b) corresponding, calculated absorption coefficient α as a function of photon energy $h\nu$. Dotted line is the fitted Drude free electron model curve, and inset shows square root of $(\alpha\text{-}\alpha_{\mathrm{Drude}})$ versus $h\nu$.

C. Optical absorption measurement

The primary goal of the optical measurements presented here is to find evidence for the indirect gap of ScN, predicted to be between 0.9 and 1.6 eV.[6,11,26] This has not been attempted previously primarily because the optical absorption due to an indirect transition is several orders of magnitudes smaller than that of the direct transition and it is therefore hard to observe experimentally. In order to increase the measurement accuracy in the present investigation, in particular in the low-absorption wavelength range, we have grown a rather thick epitaxial ScN layer on MgO(001) with a thickness of 2.5 μm.

Figure 5(a) shows the measured transmission $T(h\nu)$ and reflection $R(h\nu)$ spectra in the energy range from 0.38 to 3 eV. The oscillation in the spectra are interference fringes due to multiple reflections from the layer surface and the layer-substrate interface and indicate considerable transpar-

ency in the interval between 0.5 and 2 eV. This is perfectly consistent with the transmission data, showing a steep increase of $T(h\nu)$ around 0.5 eV and a steep decrease around 2 eV, which can be accounted for by the free carrier absorption at $h\nu < 0.5$ eV and direct interband transitions with an onset energy of 2.15 eV, respectively.[8] The reflectivity increases slightly as a function of photon energy in the transparent wavelength range and exhibits a broad peak around 2.2 eV. This is due to a small increase in the refractive index below the direct bandgap and a resonance just above the onset of interband transitions, as expected from basic oscillator theory and in agreement with previously reported optical properties of ScN.[11]

The transmission and reflection spectra were fit simultaneously using an iterative procedure which accounts for an infinite set of multiple reflections on layer surface, layer-substrate interface, and substrate back surface. The optical properties of the MgO substrate were taken from the *Handbook of Optical Constants of Solids II*.[38] Good convergence of the fit was achieved by calculating the reflection coefficients in the transparent range 0.4–2.1 eV, without accounting for the extinction coefficient k. That is, during the iterative fitting procedure the reflection coefficients at the surfaces and interfaces were calculated using a constant $k=0$, while a variable $k \geqslant 0$ was used to calculate the absorption within the layer. With this approach, the extinction coefficient and consequently also the absorption coefficient are determined solely from the intensity loss during the travel of the light through the bulk of the layer and are only to second order affected by possible surface irregularities including surface roughness or oxides. This method adds a small error of less than 0.5% to the determination of the absorption coefficient in the transparent region ($h\nu < 2$ eV), but removes all possible systematic errors due to a wrong treatment of surface effects. The fit provides values for the refractive index of ScN in the transparent range of $n=2.7-2.9$, in good agreement with the previously reported range from 2.6 to 2.8.[11]

Figure 5(b) shows the obtained absorption coefficient α as a function of photon energy $h\nu$ in the energy range $0.38 < h\nu < 2.5$ eV. α decreases with increasing photon energy down to a minimum of 8×10^2 cm^{-1} at 0.85 eV. It then increases, first slowly and then steeply, as the photon energy approaches the direct transition at 2.15 eV and reaches $\sim10^5$ cm^{-1} (outside the shown range) at 2.2 eV. The absorption minimum, 8×10^2 cm^{-1}, is 1–2 orders of magnitudes lower than previously published values ranging from 6×10^3 cm^{-1} to 3×10^4 cm^{-1} indicating the high crystalline quality of the samples used in our study.[8,11,24,27] More importantly, by acquiring optical transmission data from a rather thick layer, as described above, the accuracy of the present data in the low-absorption regime is considerably higher.

The absorption in the low photon energy range ($h\nu < 0.5$ eV) is primarily due to intraband transitions, i.e., absorption from free carriers in the conduction band. The optical properties in this energy range can be described by the Drude model, providing the following expression for the complex dielectric function $\varepsilon(\omega)$:

$$\varepsilon(\omega) = \varepsilon_\infty - \frac{\omega_p^2}{(\omega^2 + i\gamma\omega)}. \quad (1)$$

Here ω_p is the plasma frequency and $\gamma = 1/\tau$ is the Drude damping term with τ being the free electron relaxation time. ε_∞ is a constant accounting for all interband transitions as well as the core electrons. The dashed line in Fig. 5(b) is obtained by fitting the experimental data for $h\nu < 0.75$ eV with the expression in Eq. (1). The fit provides a value for plasma frequency of 2.9×10^{14} s^{-1}, which can be used to determine the free carrier concentration N using

$$\omega_p^2 = \frac{Ne^2}{\varepsilon_0 m^*}. \quad (2)$$

Using an optical effective mass m^* equal to $0.178m_e$,[37] results in a value for N of 4.8×10^{18} cm^{-3}. We attribute the charge carriers to electrons in the conduction band due to V_N's or O_N's which act as donors.[39] The carrier relaxation time, also obtained from the Drude-fit, is 7.7×10^{-15} s. This gives, using a density of states effective mass $m^* = 0.281m_e$,[37] a value for the room-temperature mobility =48 cm^2/V s.

In order to investigate interband transitions and detect a possible indirect gap, we subtract the absorption α_D due to the Drude free carriers [dashed line in Fig. 5(b)] from the measured absorption α. This difference corresponds to the absorption α_t due to interband transitions. The square root of the absorption due to an indirect transition is expected to increase linearly with photon energy. We therefore plot in the inset of Fig. 5(b) $\sqrt{\alpha_t}$ vs $h\nu$. α_t is zero for $h\nu = 0.8$ eV and increases above this value, indicating an onset for interband transitions. The $\sqrt{\alpha_t}$ plot exhibits a linear range between 0.9 to 1.7 eV consistent with an indirect transition. The extrapolation to zero intensity occurs at about 0.6 eV. The exact onset energy for the indirect transition is strongly dependent on the fitting parameters of the Drude model, and therefore contains a relatively large uncertainty also due to possible contributions of midbandgap defect states. Nevertheless, the optical absorption data indicates that there is an indirect transition within the interval of 0.6–1.1 eV. This is consistent with our STS results showing that the minimum gap in ScN is in the range 0.9–0.95 eV.

IV. CONCLUSIONS

It has been experimentally shown that both atoms Sc and N, of ScN(001) grown smoothly under N-rich conditions are resolved using STM. Based on scanning tunneling spectroscopy results, it is determined that the most prominent atom observed at low bias voltages (both positive and negative) for highly n-type ScN(001) 1×1 is the Sc atom due to the Fermi level at the surface being inside the Sc 3d band. The N atom also appears at positive sample biases due to a minority band of N 2p states in the CB. We also observe long-range topographic distortions at the surface which are attributed to the effect of charge accumulation around subsurface positively ionized dopants.

STS of the stoichiometric ScN films also shows a bandgap of ~0.9 eV, while STS of N-deficient ScN films shows a similar bandgap of ~0.95 eV as well as the second onset at ~2.2 eV. The ideal 1×1 surface is concluded to be semiconducting although the presence of additional conductance, which is attributed to the high density of electrons in the conduction band, makes the apparent gap very small. The N-deficient surface, on the other hand, is metallic. Optical absorption results for a 2.5 μm thick ScN film grown under N-rich conditions indicate indirect absorption in the range 0.9 to 1.7 eV. These results give experimental evidence for an indirect gap in ScN of 0.9 ± 0.1 eV and the direct transition at 2.15 eV.

ACKNOWLEDGMENTS

This work has been supported by the National Science Foundation under Grant No. 9983816. H. Al-Brithen acknowledges financial support from King Saud University. The authors also acknowledge useful discussions with M. E. Kordesch, S. Ulloa, and W. R. L. Lambrecht.

[1] D. Gall, I. Petrov, N. Hellgren, L. Hultman, J. E. Sundgren, and J. E. Greene, J. Appl. Phys. **84**, 6034 (1998).
[2] J.-E. Sundgren, B. O. Johansson, A. Rockett, S. A. Barnett, and J. E. Greene, *Physics and Chemistry of Protective Coatings*, edited by J. E. Greene, W. D. Sproul, and J. A. Thornton, American Institute of Physics Series No. 149 (AIP, New York, 1986), p. 149.
[3] K. Suzuki, T. Kaneko, H. Yoshida, Y. Obi, H. Fujimori, and H. Morita, J. Alloys Compd. **306** (1-2), 66 (2000).
[4] H. Yang, H. Al-Brithen, A. R. Smith, J. A. Borchers, R. L. Cappelletti, and M. D. Vaudin, Appl. Phys. Lett. **77**, 3860 (2001).
[5] H. Yang, H. Al-Brithen, E. Trifan, D. C. Ingram, and A. R. Smith, J. Appl. Phys. **91**, 1053 (2002).
[6] C. Stampfl, W. Mannstadt, R. Asahi, and A. J. Freeman, Phys. Rev. B **63**, 155106 (2001).
[7] H. A. Al-Brithen, E. M. Trifan, D. C. Ingram, A. R. Smith, and D. Gall, J. Cryst. Growth **242**, 345 (2002).
[8] A. R. Smith, H. A. H. Al-Brithen, D. C. Ingram, and D. Gall, J. Appl. Phys. **90**(4), 1809 (2001).
[9] D. Gall, I. Petrov, L. D. Madsen, J. E. Sundgren, and J. E. Greene, J. Vac. Sci. Technol. A **16**, 2411 (1998).
[10] D. Gall, I. Petrov, P. Desjardins, and J. E. Greene, J. Appl. Phys. **86**, 5524 (1999).
[11] D. Gall, M. Stadele, K. Jarrendahl, I. Petrov, P Desjardins, R. T. Haasch, T.-Y. Lee, and J. E. Greene, Phys. Rev. B **63**, 125119 (2001).
[12] N. Takeuchi, Phys. Rev. B **65**, 045204 (2002).
[13] Bernhard Eck, Richard Dronskowski, Masao Takahashi, and Shinichi Kikkawa, J. Mater. Chem. **9**, 1527 (1999).
[14] Hisashi Shimizu, Masafumi Shirai, and Naoshi Suzuki, J. Phys. Soc. Jpn. **66**, 3147 (1997).
[15] X. Bai, and M. E. Kordesch, Appl. Surf. Sci. **175-176**, 499 (2001).
[16] X. Bai, Doctoral Dissertation, Ohio University, November, 2000.
[17] W. Lengauer, J. Solid State Chem. **76**, 412 (1988).
[18] H. A. AL-Brithen and A. R. Smith, Appl. Phys. Lett. **77**(16), 2485 (2000).
[19] J. P. Dismukes and T. D. Moustakas, Proc.-Electrochem. Soc. **96-11**, 110 (1996).
[20] M. Little and M. E. Kordesch, Appl. Phys. Lett. **78**, 2891 (2001).
[21] F. Perjeru, X. Bai, M. I. Ortiz-Libreros, R. Higgins, and M. E. Kordesch, Appl. Surf. Sci. **175-176**, 490 (2001); F. Perjeru, X. Bai, and M. E. Kordesch, Appl. Phys. Lett. **80**, 995 (2002).
[22] A. Dauodi, S. Elkhattabi, G. Berthier, and J. P. Flament, Chem. Phys. **230**, 31 (1998).
[23] R. Monnier, J. Rhyner, T. M. Rice, and D. D. Koelling, Phys. Rev. B **31**, 5554 (1985).
[24] G. Travaglini, F. Marabelli, R. Monnier, E. Kaldis, and P. Wachter, Phys. Rev. B **34**(6), 3876 (1986).
[25] P. Weinberger, K. Schwarz, and A. Neckel, J. Phys. Chem. Solids **32**, 2063 (1971).
[26] W. R. L. Lambrecht, Phys. Rev. B **62**, 13 538 (2000).
[27] J. P. Dismukes, W. M. Yim, and V. S. Ban, J. Cryst. Growth **13/14**, 365 (1972).
[28] T. D. Moustakas, R. J. Molnar, and J. P. Dismukes, Proc.-Electrochem. Soc. **96-11**, 197 (1996).
[29] N. Takeuchi and S. Ulloa, Phys. Rev. B **65**, 235307 (2002).
[30] C. Stampfl, R. Asahi, and A. J. Freeman, Phys. Rev. B **65**, 161204 (2002).
[31] R. M. Feenstra, J. A. Stroscio, J. Tersoff, and A. P. Fein, Phys. Rev. Lett. **58**(12), 1192 (1987).
[32] J. A. Stroscio, R. M. Feenstra, and A. P. Fein, Phys. Rev. Lett. **58**(16), 1668 (1987).
[33] J. F. Zheng, X. Liu, N. Newman, E. R. Weber, D. F. Ogletree, and M. Salmeron, Phys. Rev. Lett. **72**(10), 1490 (1994).
[34] K.-J. Chao, A. R. Smith, and C.-K. Shih, Phys. Rev. B **53**, 6935 (1996).
[35] M. I. Ortiz-Libreros, F. Perjeru, X. Bai, and M. E. Kordesch, Appl. Surf. Sci. **175-176**, 512 (2001).
[36] R. M. Feenstra, Phys. Rev. B **50**(7), 4561 (1994).
[37] These values are obtained from Professor W. R. L. Lambrecht's calculations, who finds at the X-point CBM a longitudinal effective mass $m_l=1.441m_e$ and a transverse effective mass $m_t=0.124m_e$. For the optical effective mass, we use $3/m_{\rm opt}=1/m_l+2/m_t$, while for the DOS effective mass, we use $m_{\rm DOS}^3=m_t^2m_l$.
[38] E. D. Palik, *Handbook of Optical Constants of Solids II* (Academic, Boston, 1991), p. 950.
[39] D. Gall, I. Petrov, and J. E. Greene, J. Appl. Phys. **89**, 401 (2001).